applied sciences

MDPI

Article

Resonance Suppression of a Controllable Mechanism Welding Robot End with Central Composite Design Methodology

Yuanyuan Shi [1], Chaopeng Li [1] and Yizhe Huang [2,*]

[1] State Key Laboratory of Digital Manufacturing Equipment and Technology, Huazhong University of Science and Technology, Wuhan 430074, China; d201980200@hust.edu.cn (Y.S.); m201870534@hust.edu.cn (C.L.)
[2] School of Mechanical Engineering, Hubei University of Technology, Wuhan 430068, China
* Correspondence: yizhehuang@hbut.edu.cn

Abstract: Aiming to achieve resonance suppression of a controllable mechanism welding robot end using dynamic modeling and experimental verification, this paper applies a central composite design methodology to optimize suppression resonance using three variables: excitation source, rod stiffness and damping. Considering the coupling effects of the excitation source, member stiffness and damping, a combination optimization is carried out, and the optimal control result of the end is obtained, for which the optimized peak amplitudes are significantly reduced. The research provides an important technical basis for the dynamic design and resonance suppression control of controllable welding robot mechanisms.

Keywords: suppression resonance; welding robot; central composite design methodology; combination optimization

check for updates

Citation: Shi, Y.; Li, C.; Huang, Y. Resonance Suppression of a Controllable Mechanism Welding Robot End with Central Composite Design Methodology. *Appl. Sci.* **2022**, *12*, 6352. https://doi.org/10.3390/app12136352

Academic Editor: Alessandro Gasparetto

Received: 8 June 2022
Accepted: 19 June 2022
Published: 22 June 2022

Publisher's Note: MDPI stays neutral with regard to jurisdictional claims in published maps and institutional affiliations.

Copyright: © 2022 by the authors. Licensee MDPI, Basel, Switzerland. This article is an open access article distributed under the terms and conditions of the Creative Commons Attribution (CC BY) license (https://creativecommons.org/licenses/by/4.0/).

1. Introduction

Welding is an essential part of manufacturing industry, and welding robots are widely used to decrease costs, improve quality and increase productivity in which quality is one of the most important considerations in the welding process [1–4]. In the process of operation, vibration inevitably occurs in the welding robot system due to multi-source excitation such as the motor drive and welding gun impact vibration. The vibration level of the welding robot directly affects the welding quality [5], and the suppression of resonance has become an important research direction [6–8]. Therefore, controlling the suppression resonance is an important consideration in the design and development of welding robots [9,10]. During the working process of welding robots, several motors are often required to operate at the same time to realize the complex trajectory of the welding. As the driving source of motion, the motor at the joint mechanism is also an excitation source for system vibration. The posture change of the robot mechanism during welding leads to a dynamic change of the modal performance. The dynamic mode is more likely to cause mode resonance under the action of multi-source excitation, which seriously affects the welding accuracy at the end of the gun. Therefore, the vibration optimization of the mechanism or structure is the basis for achieving high-performance work goals in the machine system, i.e., the moment of the motor, stiffness and damping of the mechanism are important inherent characteristics of the robot system which become important parameters in the influence of vibration on welding accuracy. Scholars pay greater attention to the study of vibration optimization control of traditional structures [11–13]. However, due to the complex excitation sources and changing motion posture, the vibration optimization control of controllable mechanism of welding robots requires relatively little calculation or few test groups to establish a model closer to the actual situation. The response surface method enables parameter optimization [14–21].

Central composite design (CCD) methodology is a well-adapted statistical test design method. The principle is to create a surface model of continuous variables by searching

for quantitative rules between test indexes and various factors. Built on the evaluation of the factors and their interaction, the optimal level range of each factor is found, and the number of calculations or test groups is relatively small. Because of the complex multi-dimensional surface, it is more faithful to the actual situation, and can be used extensively to solve complex problems such as the optimal proportion of materials and multi-factor optimization [22,23]. At present, a small number of scholars have applied this method in the field of mechanical formula design [24,25]. The central composite design methodology itself is based on parameter optimization, which means it has broad application prospects in the suppression resonance parameter optimization of controllable mechanism welding robots.

2. Optimization Design Method

2.1. Dynamic Modeling and Validation

The object of this paper is a controllable mechanism welding robot, and the prototype and model of the controllable mechanism welding robot are shown in Figure 1.

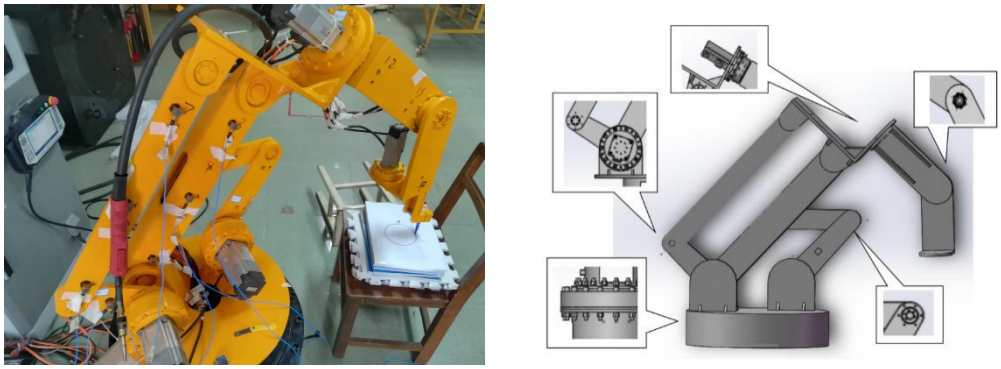


Figure 1. The prototype and model of the controllable mechanism welding robot.

To verify the feasibility of the vibration optimization of the response surface method at the end of the controllable mechanism welding robot, the simulation model was verified by a modal test.

The test system includes a welding robot test stand, an attitude control system, an excitation system, a spectrum acquisition system and a modal analysis system. A single point excitation multi-point response test scheme is utilized. The validation scheme takes the mechanism part of the welding robot as the object and controls the system to the welding posture. The force hammer (LMS 086c03) collects the excitation signal and the PCB acceleration three-way sensor (ICP 365A25 series) collects the acceleration signal at several measuring points. The excitation signal and vibration acceleration signal obtained by the LMS test system are used to analyze the transfer function between the excitation point and the measuring point. Finally, the modal information of the tested structure is extracted in Poly Max and verified with the simulation mode in this study. The experimental site and scheme are shown in Figure 2.

A comparison of the first seven natural frequencies between the simulation and tests is shown in Table 1.

Taking the vibration mode diagram of the first four modes in Table 1 as an example, the modal vibration mode diagrams for the simulation analyses and tests are shown in Figures 3–6, respectively.

Table 1 shows that the error rate between the simulated and tested modal frequencies is within 10%. Figures 3–6 indicate that the simulated mode shapes are similar to the tested modes. These results show that the modal simulation and tests of the controllable mechanism welding robot have high consistency, which verifies the correctness of the simulation model and lays a reliable foundation for further vibration optimization research.

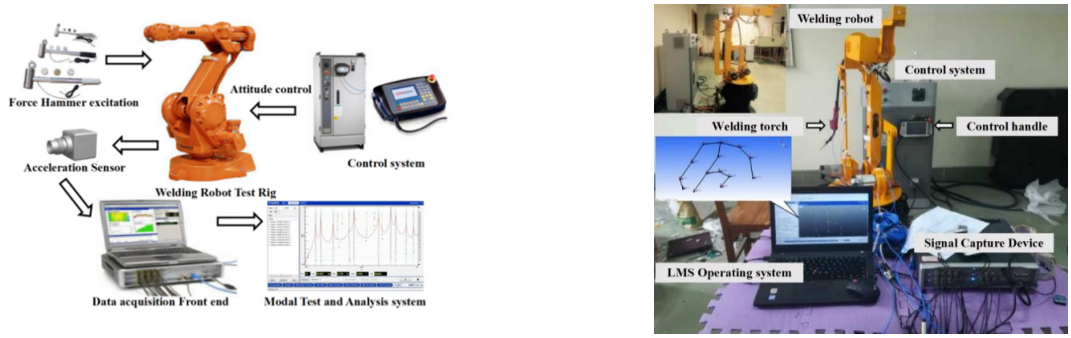


Figure 2. Experimental system for verification.

Table 1. Comparison of the first seven natural frequencies between the simulations and tests.

Order	Simulation Result (Hz)	Experimental Result (Hz)	Error Rate
1	10.27	9.415	9.081%
2	15.917	16.504	3.557%
3	18.162	17.376	4.523%
4	37.23	37.105	0.337%
5	46.456	42.683	8.840%
6	54.059	52.658	2.661%
7	80.016	83.801	4.517%

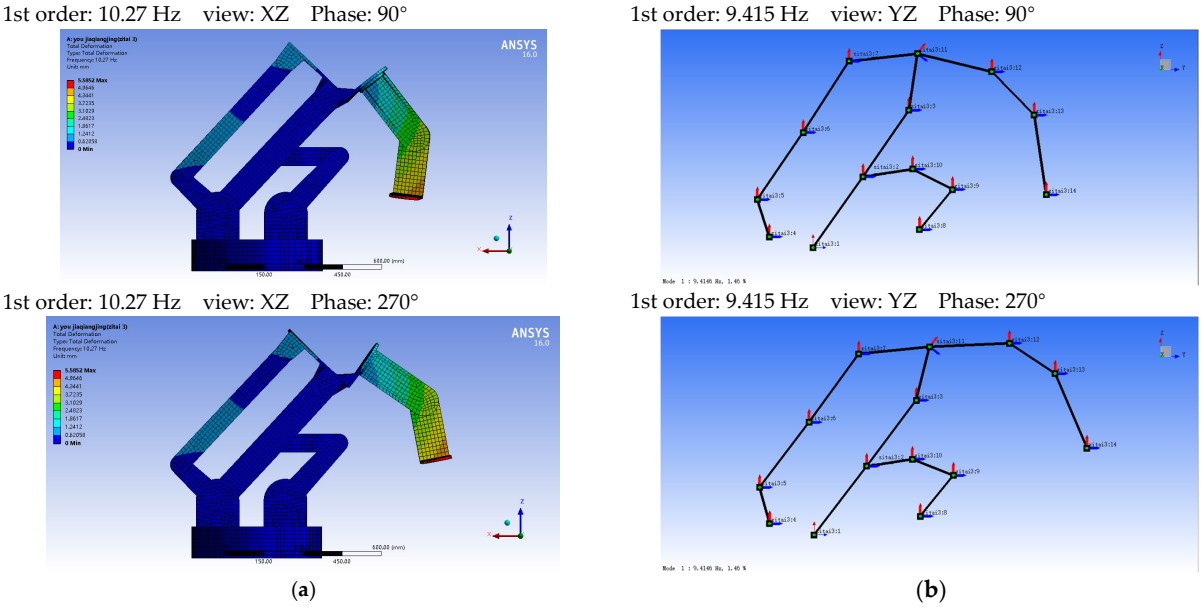


Figure 3. (**a**) First-order simulation mode diagram; (**b**) First-order test mode diagram.

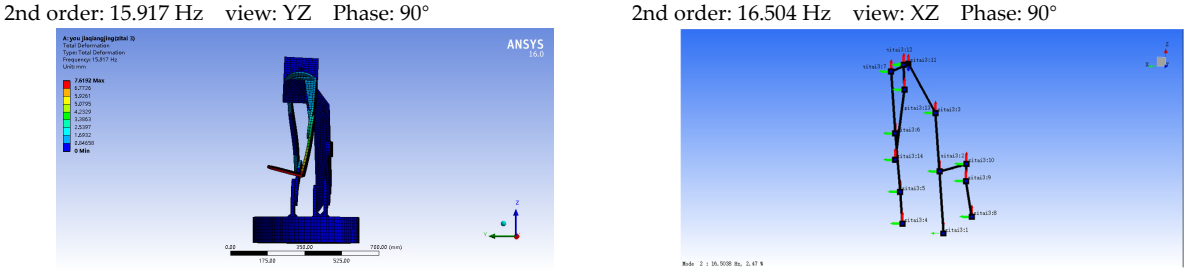


Figure 4. *Cont.*

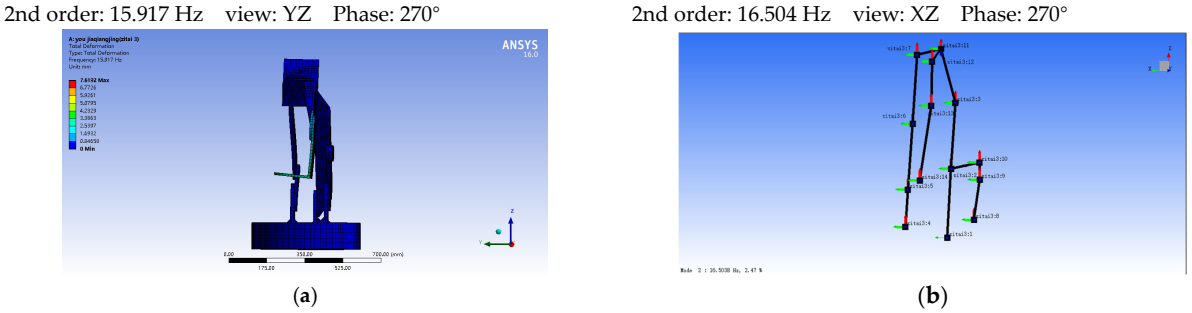


Figure 4. (**a**) Second-order simulation mode diagram; (**b**) Second-order test mode diagram.

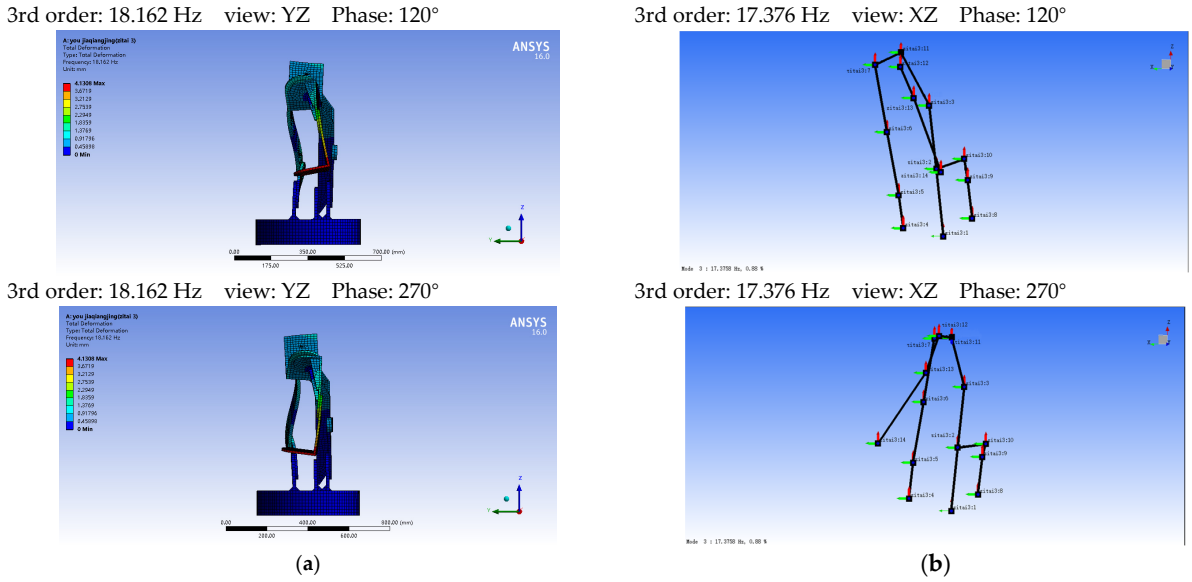


Figure 5. (**a**) Third-order simulation mode diagram; (**b**) Third-order test mode diagram.

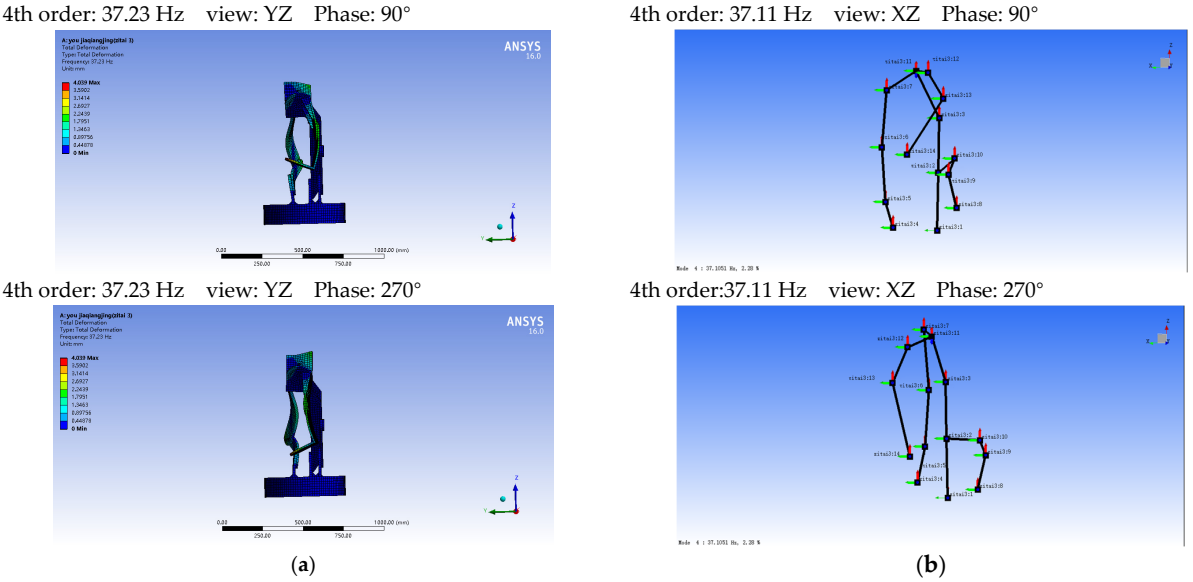


Figure 6. (**a**) Fourth-order simulation mode diagram; (**b**) Fourth-order test mode diagram.

2.2. Central Composite Design Methodology for Vibration Optimization

To determine the interaction between the vibration factors caused by the controllable mechanism welding robot and to study the comprehensive effect of each factor on the dynamic performance of the controllable mechanism welding robot, the CCD method is used to optimize the welding accuracy of the welding torch at the end of the controllable mechanism welding robot. The CCD and BBD depicted in Figure 7 show that many points of the CCD method will exceed the original level, which enables the CCD method to better fit the corresponding surface [15]. A surface model of the vibration response of each factor and the welding torch at the end of controlled mechanism welding robot is established by a design simulation test. The optimum target and the optimum ascending direction are determined to solve the optimum parameters of the vibration attenuation target of the welding end, so as to realize the vibration optimization of the welding end of the controlled mechanism welding robot. The design steps of the CCD methodology of the end of the controllable mechanism welding robot are as follows:

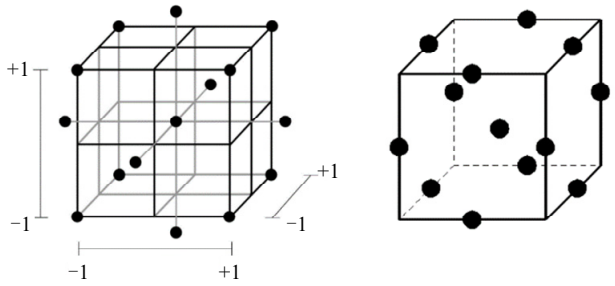


Figure 7. Central composite design (CCD) and Box-Behnken design (BBD).

Step 1: Determine the experimental design method. At present, the most frequently used experimental design methods are the CCD method and the Box-Behnken experimental design (BBD) method. Compared with the Box-Behnken experimental design method, the CCD method can better fit the corresponding surface, and it is more suitable for multi-factor and multi-level experiments with continuous variables. Based on the assumption that there are many factors involved in the vibration problem of the welding robot mechanism, the CCD method was selected for the experimental design in this paper.

Step 2: Design the test data sheet and carry out simulation calculations. According to the relationship diagram between the factors and sub-factors of the controllable mechanism welding robot, the central composite design data table is designed, the vibration harmonic response calculation of the actuator, and nonlinear data fitting are carried out. On this basis, the surface equation under the data is obtained. The obtained surface equation is subjected to error analysis to check the fitting effect and the feasibility of the equation.

Step 3: Parameter optimization design. Using Minitab software, the factors, sub-factors intervals, and optimization target values are set at the front end, and the 3D model diagram of the output under constraints is calculated and drawn, and the corresponding equations and extreme values are obtained to complete the optimization of the test results.

Figure 8 shows the flow chart of the experimental design:

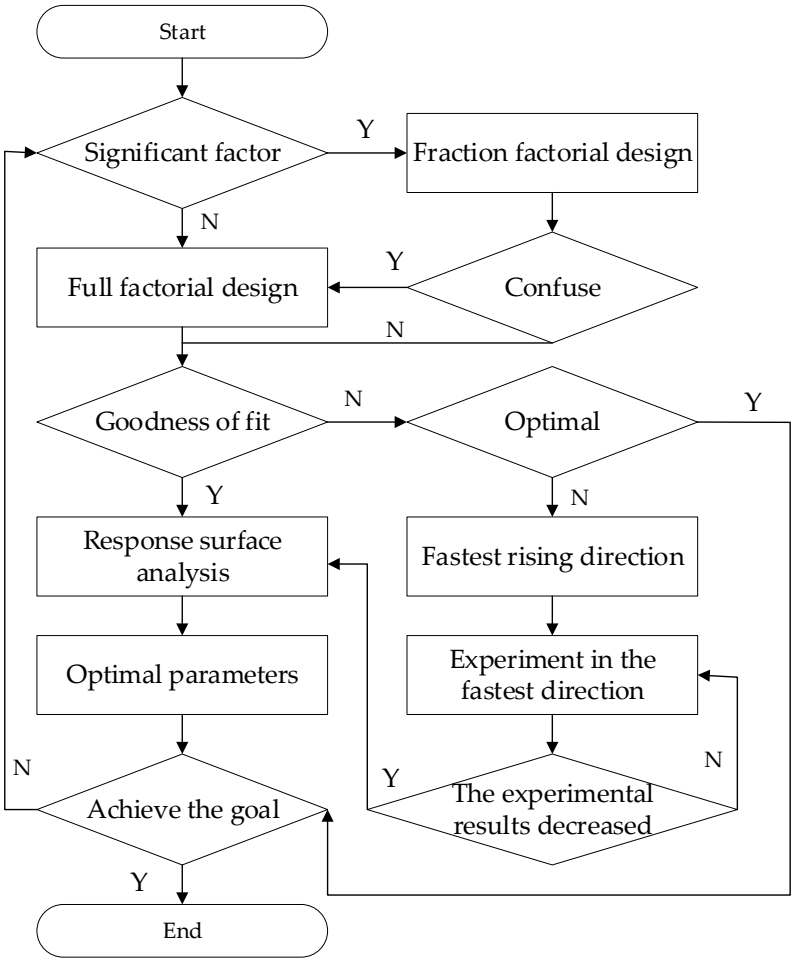


Figure 8. General flow of experimental design.

2.3. Central Composite Design

2.3.1. Design of Excitation Source Size and Location

The distribution of the excitation sources of the controllable mechanism welding robot prototype is shown in Figure 9.

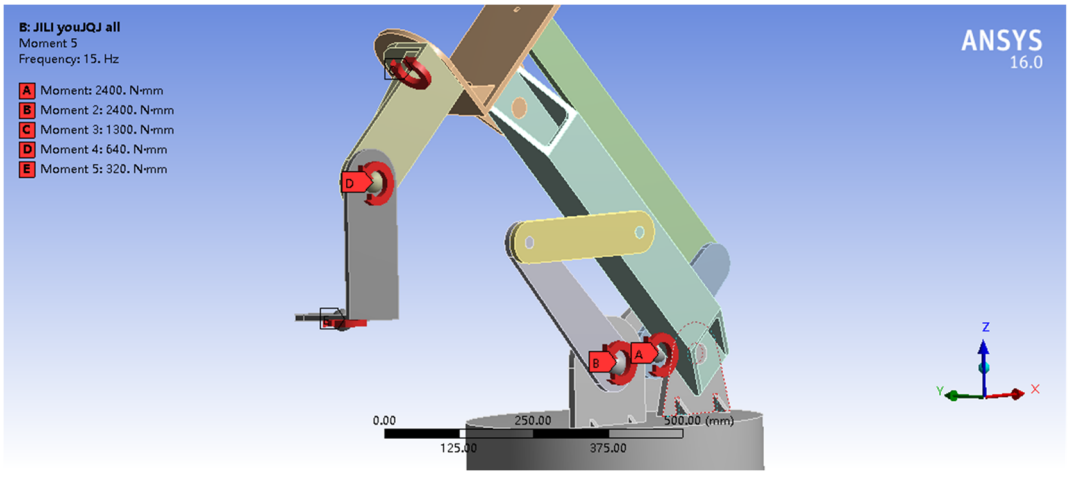


Figure 9. The distribution of excitation sources.

The positions of the excitation sources in the model are the positions of the five servo motors. The torque of A and B near the bottom of the base is 2400 N·mm; the torque of C near the connection between the rotating arm and the swing arm g is 1300 N·mm; the torque of D at the connection between the swing arm g and the end g is 640 N·mm; and the torque of E at the end g is 320 N·mm.

The design table of this test scheme consists of five factors and two levels (the five factors are represented by Moment 1, Moment 2, Moment 3, Moment 4 and Moment 5, respectively), and a group of 33 CCD experiments are designed. The data design table is provided in Table 2.

Table 2. Center composite design experimental data design of excitation sources.

Order	Moment (N·mm)					Order	Moment (N·mm)				
	1	2	3	4	5		1	2	3	4	5
1	2200	2600	1100	620	300	18	2400	2000	900	640	320
2	2200	2200	1100	620	340	19	2000	2000	1300	640	320
3	2200	2200	1100	660	300	20	2000	2400	900	600	280
4	1800	2200	1100	620	300	21	2000	2400	1300	640	280
5	2200	2200	1100	580	300	22	2200	2200	1100	620	300
6	2600	2200	1100	620	300	23	2400	2400	900	640	280
7	2200	2200	1100	620	260	24	2000	2400	1300	600	320
8	2200	2200	700	620	300	25	2000	2400	900	640	320
9	2200	2200	1500	620	300	26	2400	2400	1300	600	280
10	2200	1800	1100	620	300	27	2200	2200	1100	620	300
11	2200	2200	1100	620	300	28	2200	2200	1100	620	300
12	2000	2000	1300	600	280	29	2000	2000	900	640	280
13	2400	2000	1300	640	280	30	2400	2400	900	600	320
14	2200	2200	1100	620	300	31	2200	2200	1100	620	300
15	2400	2000	900	600	280	32	2000	2000	900	600	320
16	2200	2200	1100	620	300	33	2400	2400	1300	640	320
17	2400	2000	1300	600	320						

Using the design table, we can know the torque of the five excitation sources in each simulation test, set the torque parameters in the prototype simulation model in turn, and analyze the harmonic response.

2.3.2. Design of Bar Thickness

The components of the controllable mechanism welding robot studied are shown in Figure 10.

The harmonic response analysis of the prototype model shows that the bar thickness change has a significant impact on the amplitude value of the execution end, which connects rod 2, the swing arm g and end g. Therefore, the optimization design is carried out based on three factors: connecting rod 2, swing arm g and end g. The experimental design table adopts three factors and two levels (the three factors are represented by connecting rod 2, swing arm g and end g, respectively), and a group of 20 CCD experiments are designed. The data design table is shown in Table 3.

According to the 20 groups of experimental design schemes in Table 3, the thicknesses of connecting rod 2, swing arm g and end g are adjusted in the model while the other structural parameters are kept unchanged. The harmonic response analysis is then conducted for each design.

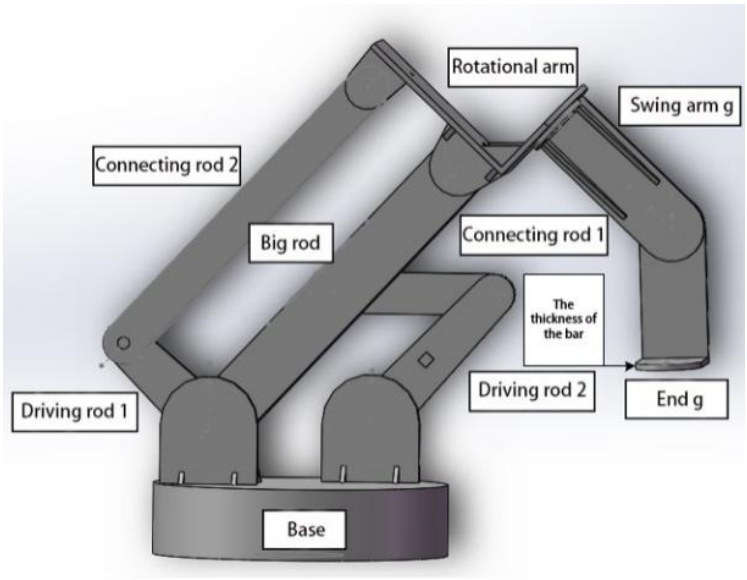


Figure 10. Series-parallel controllable mechanism welding robot component names.

Table 3. Center composite design experimental data design table of bar thickness.

Order	Connecting Rod 2 (mm)	Swing Arm g (mm)	End g (mm)	Order	Connecting Rod 2 (mm)	Swing Arm g (mm)	End g (mm)
1	14	9	10.633	11	12	8	8
2	14	9	9	12	12	8	10
3	14	7.367	9	13	12	9	9
4	14	9	7.367	14	14	9	9
5	14	9	9	15	16	10	10
6	17.266	9	9	16	12	10	10
7	14	10.633	9	17	14	9	9
8	10.735	9	9	18	14	8	10
9	12	10	8	19	16	8	8
10	16	10	8	20	14	9	9

2.3.3. Design of Damping

The harmonic response analysis of the prototype simulation model shows that the driving rod 1, connecting rod 1 and end g are the most sensitive to damping. Therefore, the optimization design is carried out based on the three factors of the driving rod 1, connecting rod 1 and the end g. The test design table adopts three factors and two levels (the three factors are represented by driving rod 1, connecting rod 1 and end g respectively), as shown in Table 4. A CCD test with a total of 20 tests was performed.

Table 4. Center composite design experimental data design table of damping values.

Order	Driving Rod 1	Connecting Rod 1	End g	Order	Driving Rod 1	Connecting Rod 1	End g
1	0.0020	0.0260	0.0260	11	0.0113	0.0407	0.0407
2	0.0260	0.0020	0.0260	12	0.0113	0.0113	0.0113
3	0.0260	0.0260	0.0260	13	0.0407	0.0407	0.0113
4	0.0260	0.0260	0.0500	14	0.0113	0.0407	0.0113
5	0.0260	0.0260	0.0260	15	0.0407	0.0113	0.0407
6	0.0260	0.0500	0.0260	16	0.0260	0.0260	0.0260
7	0.0500	0.0260	0.0260	17	0.0407	0.0113	0.0113
8	0.0260	0.0260	0.0020	18	0.0260	0.0260	0.0260
9	0.0113	0.0113	0.0407	19	0.0260	0.0260	0.0260
10	0.0407	0.0407	0.0407	20	0.0260	0.0260	0.0260

The damping value of each member of the original model of the prototype is treated as undamped. According to the 20 groups of data in Table 4, the damping values of the corresponding driving rod 1, connecting rod 1 and end g in the original model are set. Under the condition that other steps remain unchanged, the amplitude frequency curve of the end displacement value of the controllable mechanism welding robot can be obtained by the simulation calculation.

3. Results and Discussion

3.1. Optimal Parameters for the Size and Position of the Excitation Source

The simulation calculation shows that the vibration displacement in the Y direction of the execution end is the largest, and the maximum amplitude of the execution end of the original model is 0.5838 mm. The results obtained with the settings in Table 1 show that the maximum vibration amplitude of the execution end is found at 16 Hz. The corresponding main effect diagrams and interaction diagrams are shown in Figures 11 and 12, respectively. The main effects plot (Figure 11) compares the difference between the horizontal means of the torque of the five motors. The horizontal coordinates are the variation level of each motor's torque, and the longitudinal coordinates are the differences of the response means. The interaction plot (Figure 12) illustrates how the relationship between one moment and the continuous response depends on the value of another moment. This figure shows the horizontal mean of one torque on the *x*-axis and a separate line for each level of the other torque.

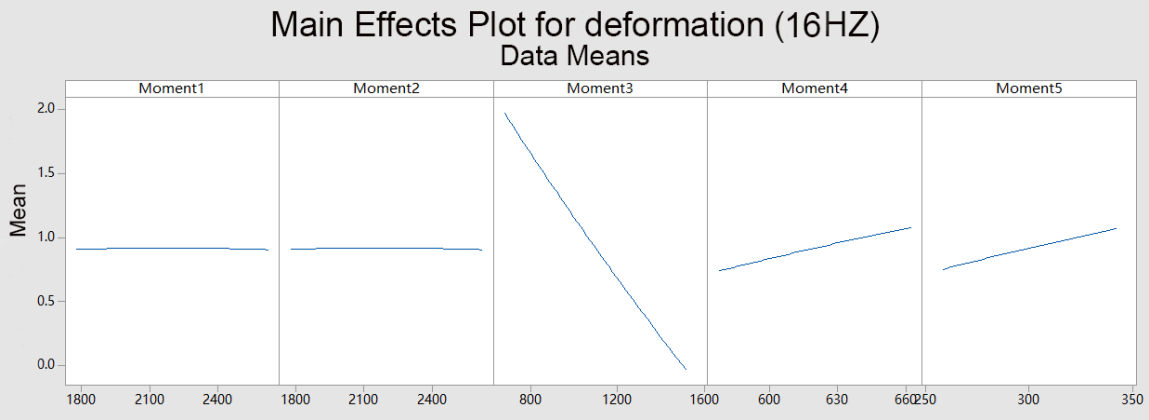


Figure 11. Main effect diagrams of maximum amplitude displacement at the end of a series-parallel controllable mechanisms welding robot.

Figures 11 and 12 indicate that Moment 3 has the most significant influence on the amplitude displacement value at the end of the controllable mechanism welding robot, whereas Moment 1 and Moment 2 have no effect, and Moment 4 and Moment 5 have no significant effect.

The optimization target of the amplitude displacement value of the execution end is set to 0 mm, and solved using the response optimizer in Minitab. The resulting optimization plot is shown in Figure 13.

The optimization graphic results in Figure 13 are provided in table form in Table 5.

Figure 13 and Table 5 show that when Moment 1 to Moment 5 are 2400 N·mm, 2400 N·mm, 1300 N·mm, 600 N·mm and 280 N·mm, respectively, the amplitude response displacement of the end of the controllable mechanism welding robot is at a minimum. Compared with the initial amplitude response displacement of 0.5838 mm, the amplitude response displacement decreases by 51%.

The amplitude response curve of the execution end obtained after optimization is shown in Figure 14.

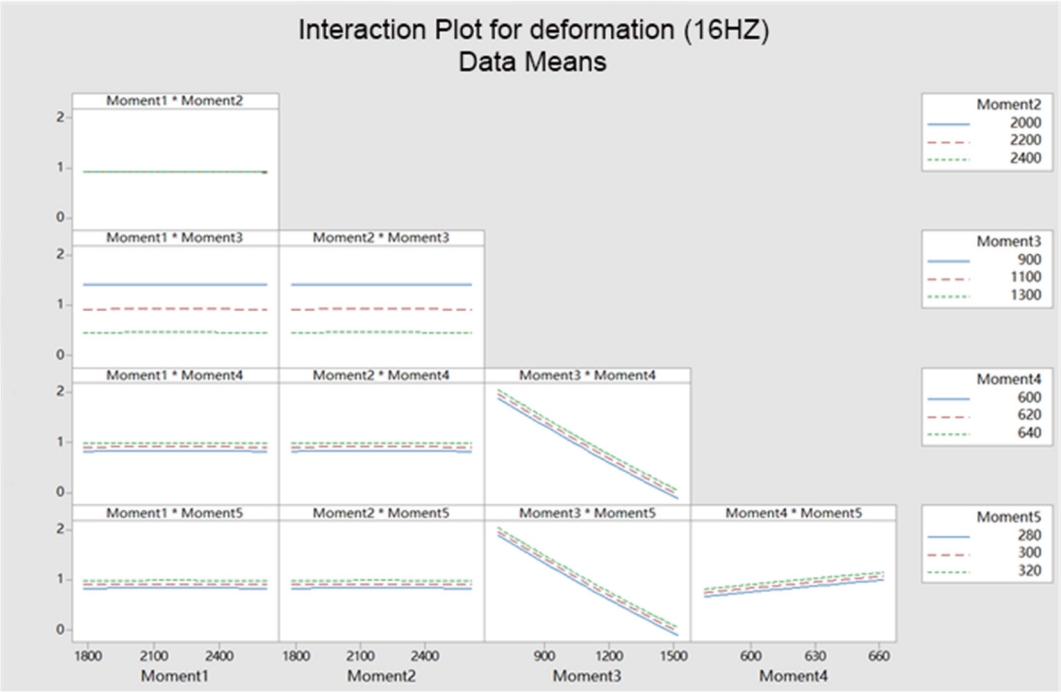


Figure 12. Interaction diagrams of the maximum amplitude displacement at the end of a series-parallel controllable mechanism welding robot (The sign * in the figure means the interaction of two factors).

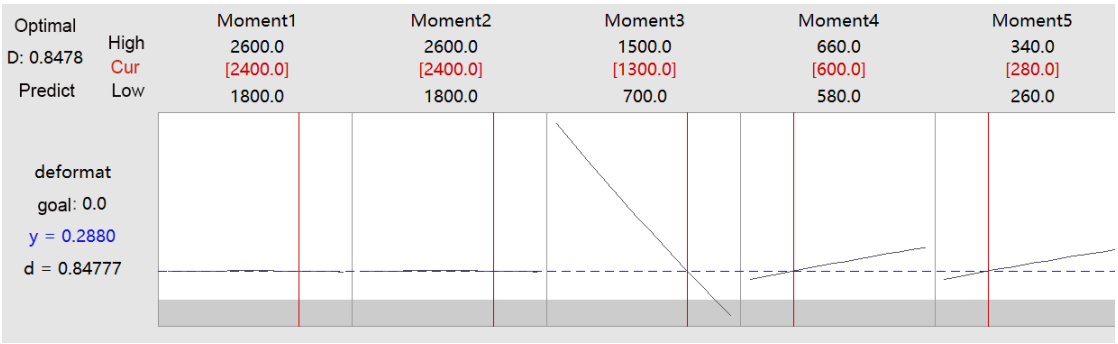


Figure 13. Response optimizer optimization diagram of excitation design.

Table 5. Response optimizer optimization results of excitation design.

Response	Fitting Value	Fitting Value Error	95% Confidence Interval	95% Prediction Interval
Deformation (16 Hz)	0.2880	0.0191	(0.2459, 0.3301)	(0.2266, 0.3495)

Figure 14 reveals that when the excitation frequency is 16 Hz, the amplitude value of the actuator end is the largest, which is close to the optimization result of the response surface methodology of 0.2880 mm. The value is within the 95% confidence interval, which means that the response surface methodology is effective for the vibration optimization of the actuator end.

3.2. Optimal Parameters of Bar Thickness

The simulation calculation is carried out according to the 20 test schemes in Table 2. The results show that the amplitude displacement value in the Y direction is the largest, and the maximum harmonic response displacement value of the controllable mechanism welding robot's execution end occurs at different frequencies: 16 Hz, 18 Hz, 24 Hz, 25 Hz,

and 45 Hz. The corresponding main effect diagrams and interaction diagrams are shown in Figures 15 and 16, respectively.

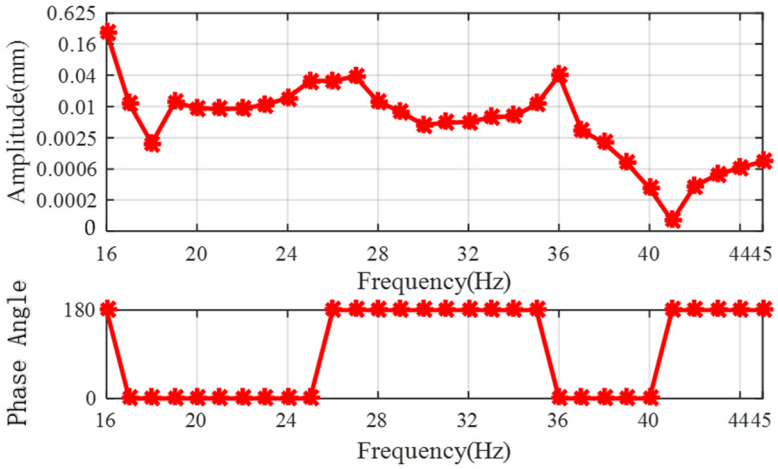


Figure 14. Amplitude response curve of the terminal surface after excitation optimization.

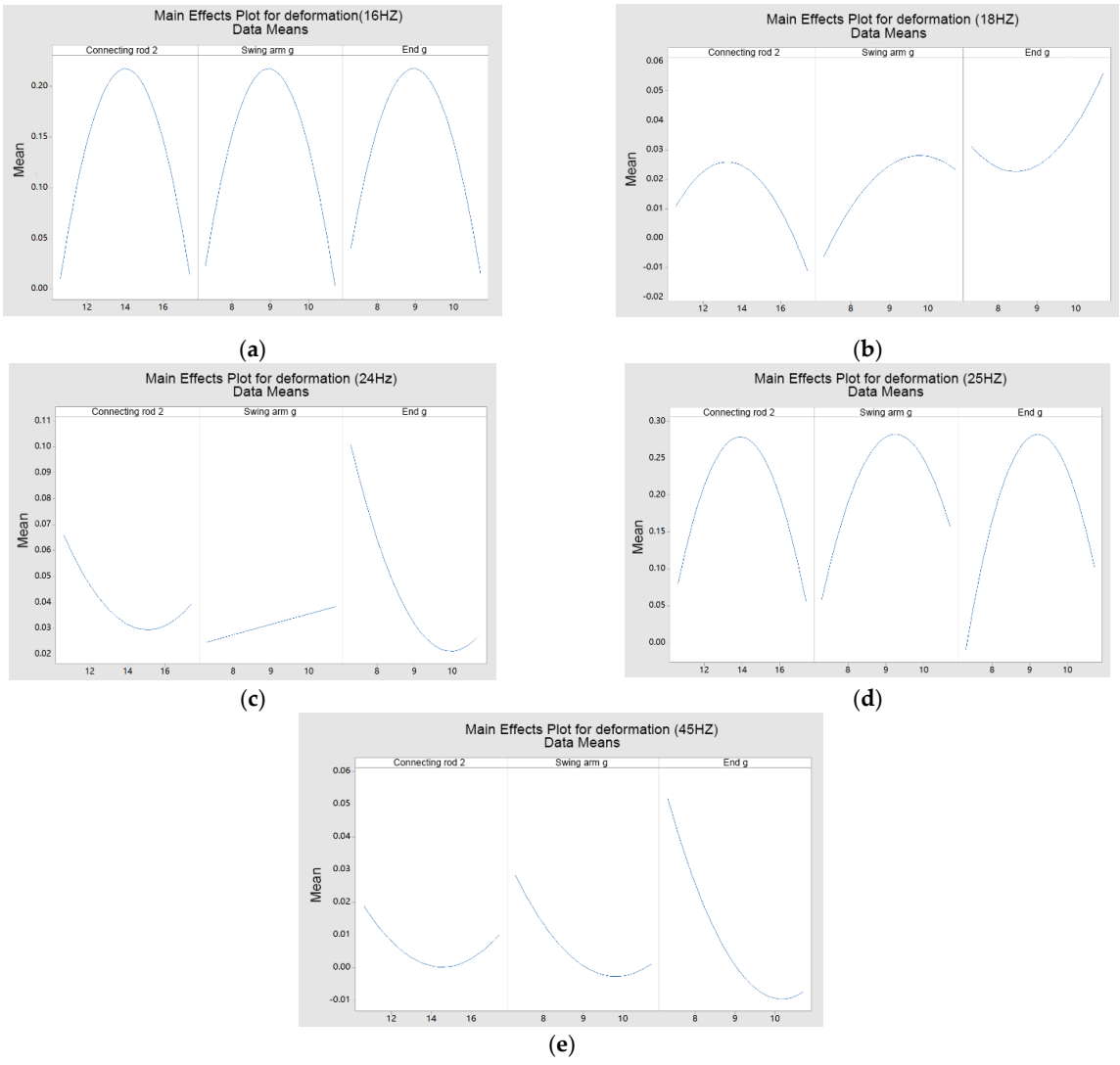


Figure 15. Main effect diagrams for the maximum amplitude displacement at the end of welding robot: (**a**) 16 Hz;(**b**) 18 Hz; (**c**) 24 Hz; (**d**) 25 Hz; (**e**) 45 Hz.

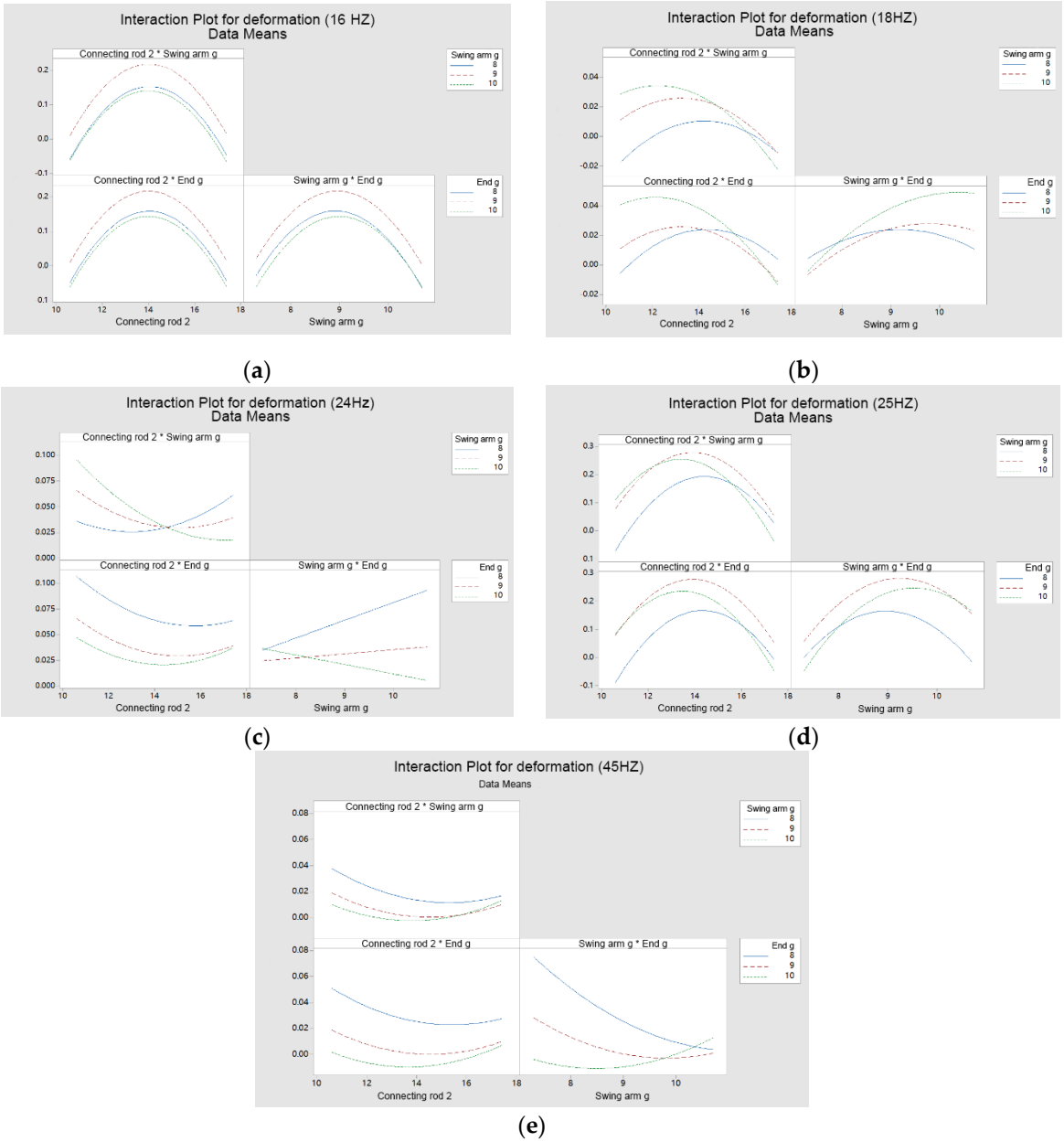


Figure 16. Interaction diagrams for the amplitude displacement at the end of the welding robot: (**a**) 16 Hz; (**b**) 18 Hz; (**c**) 24 Hz; (**d**) 25 Hz; (**e**) 45 Hz. (The sign * in the figure means the interaction of two factors).

Considering Figures 15 and 16, it can be seen that the thickness of the rod at the end g has the greatest influence on the amplitude and displacement value of the execution end of the welding robot, and the thickness of the rod at the connecting rod 2 and the swing arm g have some influence on the amplitude and displacement of the execution end.

Taking the execution end amplitude displacement value of 0 mm as the optimization target, the optimization is carried out through the response optimizer, and the optimization result is shown in Figure 17.

The optimization results in Figure 17 are shown in Table 6.

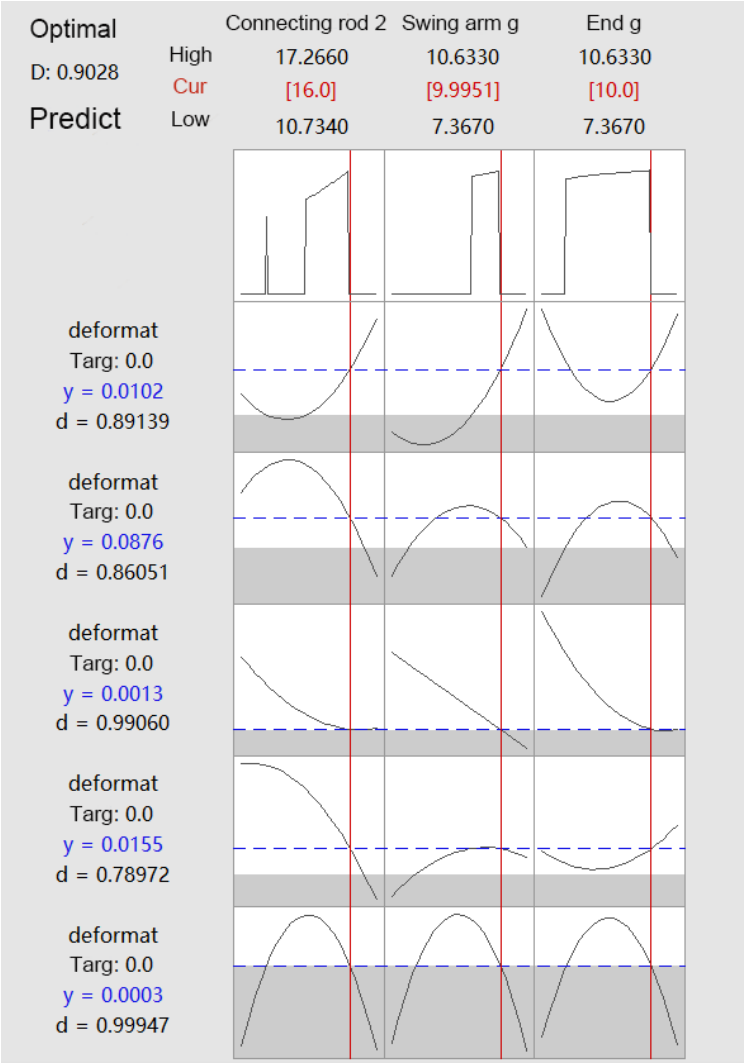


Figure 17. Optimization diagram of bar thickness design.

Table 6. Response optimizer optimization results of bar thickness design.

Response	Fitting Value	Fitting Value Error	95% Confidence Interval	95% Prediction Interval
Deformation (16 Hz)	0.0003	0.1220	(−0.2760, 0.2770)	(−0.4350, 0.4360)
Deformation (18 Hz)	0.0155	0.0147	(−0.0177, 0.0487)	(−0.0367, 0.0677)
Deformation (24 Hz)	0.0013	0.0139	(−0.0303, 0.0328)	(−0.0483, 0.0509)
Deformation (25 Hz)	0.0876	0.1450	(−0.2410, 0.4160)	(−0.4290, 0.6040)
Deformation (45 Hz)	0.0102	0.0133	(−0.0200, 0.0404)	(−0.0373, 0.0578)

As depicted in Figure 17 and Table 6, the target of the amplitude displacement at the end of welding execution is 0 mm at 16 Hz, 18 Hz, 24 Hz, 25 Hz and 45 Hz. The optimal result is achieved when the thicknesses of the connecting rod 2, swing arm g and end g are 16.0 mm, 9.9951 mm and 10 mm, respectively, and the end displacement value of the controllable mechanism welding robot is the target value. The displacement values at 16 Hz, 18 Hz, 24 Hz, 25 Hz and 45 Hz are 0.0003 mm, 0.0155 mm, 0.0013 mm, 0.0876 mm, and 0.0102 mm, respectively. Compared with the initial amplitude response displacement, the displacement is 0.0150 mm, 0.0041 mm, 0.0336 mm, 0.0302 mm, and 0.0942 mm, respectively. After optimization, the amplitude response displacement decreases by 98%, 74%, 96%, 66%, and 89%, respectively.

The amplitude response curve of the execution end obtained after optimization is shown in Figure 18.

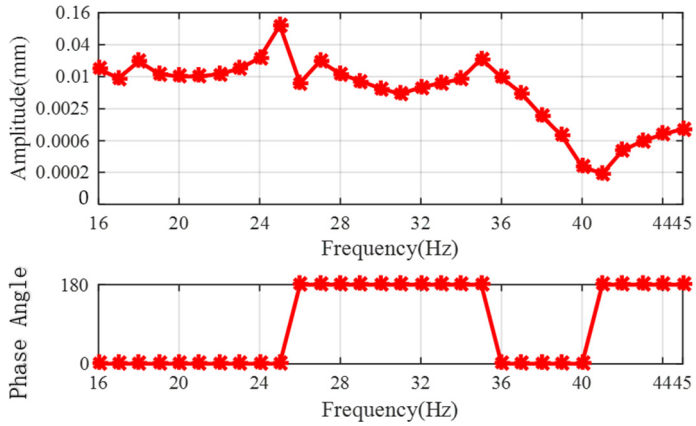
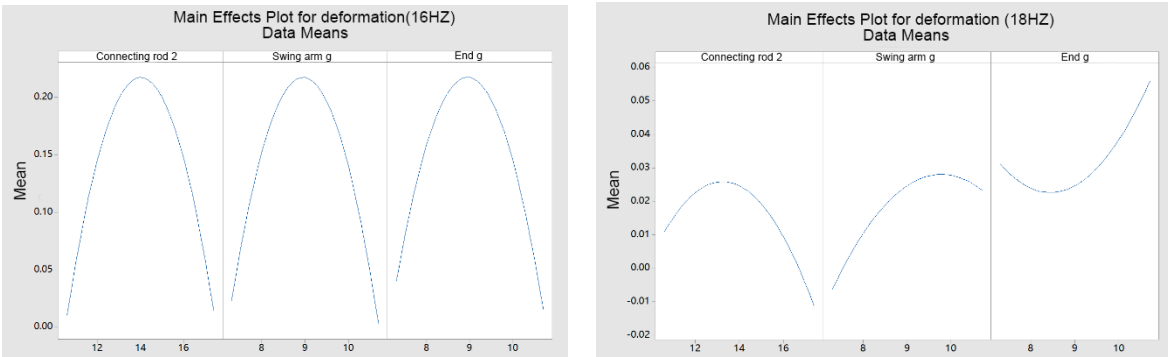


Figure 18. Amplitude response curve of the terminal surface after the optimization of the bar thickness.

The results in Figure 18 illustrate that when the excitation frequency is 25 Hz, the amplitude value of the execution end is the largest at 0.0922 mm. In Table 5, the response amplitude at 25 Hz based on the response optimization solver is 0.0876 mm. The optimized simulation calculation results are within the confidence interval of the optimization solver's solution results, so the optimization results are reasonable and accurate.

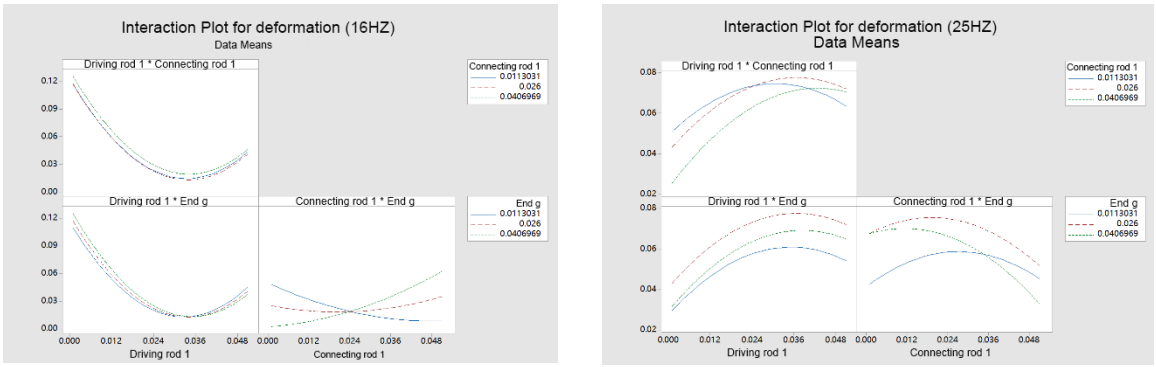
3.3. Optimal Parameters of Member Damping

The damping value of each member of the original model is treated as undamped. The damping values of driving rod 1, connecting rod 1 and end g in the original model are set according to the 20 groups of data in Table 3. Under the condition that other steps remain unchanged, the amplitude frequency curve of the displacement value of the controllable mechanism welding robot end can be obtained by the simulation calculation. The simulation results demonstrate that the vibration amplitude in the Y direction is the largest. The maximum vibration displacement amplitude of the end harmonic response of the controllable mechanism welding robot actuator occurs at two frequencies: 16 Hz and 25 Hz. The corresponding main effect diagrams and interaction diagrams are shown in Figures 19 and 20, respectively.



(**a**) (**b**)

Figure 19. The main effect diagrams of the maximum displacement at the end: (**a**) 16 Hz; (**b**) 18 Hz.



(**a**) (**b**)

Figure 20. Interaction diagrams of the amplitude displacement at the end of the welding robot: (**a**) 16 Hz; (**b**) 18 Hz. (The sign * in the figure means the interaction of two factors).

As seen in Figures 19 and 20, the damping value of driving rod 1 has the greatest impact on the end displacement value of the controllable mechanism welding robot, whereas the damping value of connecting rod 1 and end G has some impact on the end amplitude displacement value of the actuator.

Taking the end amplitude displacement value of the controllable mechanism welding robot 0 mm as the optimization target, the optimization results are shown in Figure 21.

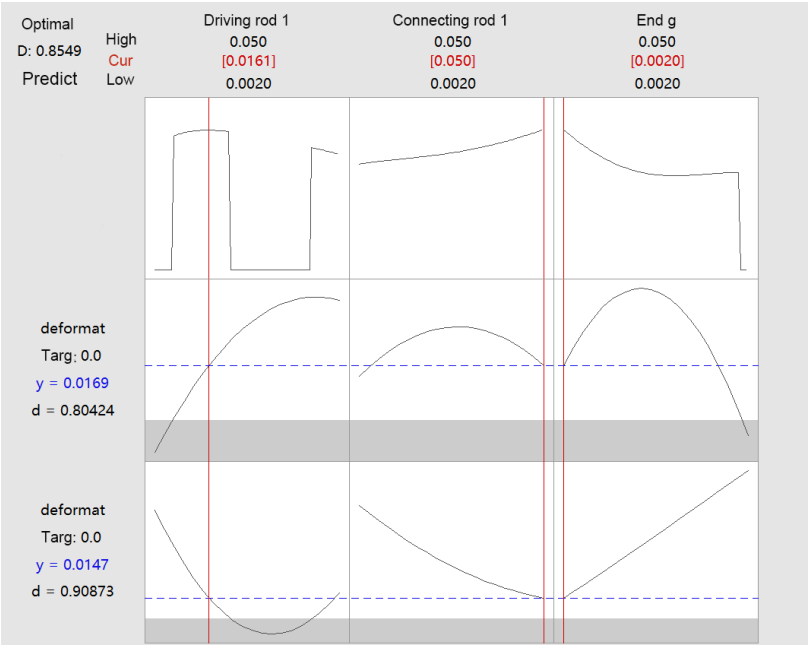


Figure 21. Optimization diagram of member damping design.

The results shown in Figure 21 are detailed in Table 7.

Table 7. Response optimizer optimization results of member damping design.

Response	Fitting Value	Fitting Value Error	95% Confidence Interval	95% Prediction Interval
Deformation (16 Hz)	0.0147	0.0433	(−0.0833, 0.1127)	(−0.1025, 0.1319)
Deformation (25 Hz)	0.0169	0.0164	(−0.0203, 0.0541)	(−0.0276, 0.0614)

The results presented in Figure 21 and Table 7 indicate that if the target end displacement of the actuator of the studied welding robot prototype is 0 mm at 16 Hz and 25 Hz,

the optimal result is obtained when the damping values of driving rod 1, connecting rod 1 and end g are 0.0161, 0.050 and 0.0020, respectively, and the vibration displacement amplitudes of the actuator end are 0.0147 mm and 0.0169 mm, respectively. Compared with the initial amplitude response displacement, the displacement is 0.1615 mm and 0.0309 mm, respectively. The amplitude response displacement is reduced by 91% and 45%, respectively, after optimization.

The optimized parameters are substituted into the simulation model for calculation, and the maximum displacement amplitude of the actuator end at 16 Hz frequency is 0.018 mm, which is consistent with the optimization result of the response optimization solver.

3.4. Optimal Parameters Considering the Excitation Source, Rod Thickness and Damping

As mentioned in Sections 3.1–3.3, the three factors of excitation source, Moment 3, the thickness of end g bar and the damping value of driving rod 1 have the greatest influence on the end displacement amplitude. Therefore, when comprehensively exploring the optimal design of the excitation source, rod thickness and damping value on the end vibration of the welding robot actuator, these three factors are used in the central composite design for optimal design.

This test adopts three factors and two levels (the three factors are Moment 3, end g thickness and damping value of driving rod 1, respectively), and a set of 20 central composite design (CCD) tests are performed. The resulting data are shown in Table 8.

Table 8. Synthesis center composite design test data design table.

Order	Moment 3 (N·mm)	Thickness of End g (mm)	Damping Value of Driving Rod 1	Order	Moment 3 (N·mm)	Thickness of End g (mm)	Damping Value of Driving Rod 1
1	1300	8	0.0500	11	1100	9	0.0260
2	1300	8	0.0020	12	1100	9	0.0260
3	900	10	0.0500	13	1100	10.633	0.0260
4	900	10	0.0020	14	773.4	9	0.0260
5	1100	9	0.0260	15	1100	9	0.0260
6	1100	9	0.0260	16	1100	9	0.0652
7	1300	10	0.0020	17	1100	9	0.0260
8	900	8	0.0500	18	1100	7.367	0.0260
9	900	8	0.0020	19	1426.6	9	0.0260
10	1300	10	0.0500	20	1100	9	0.0260

The maximum end harmonic response displacement amplitude of the actuator of the controllable mechanism welding robot occurs at multiple frequencies of 16 Hz, 18 Hz, 25 Hz and 43 Hz. Taking the vibration end amplitude displacement value of 0 mm as the optimization goal, the optimization results obtained through the response optimizer are shown in Figure 22.

The optimization results of Figure 22 are detailed in Table 9.

As can be seen from Figure 22 and Table 9, when the target displacement amplitude of the actuator end is 0 mm at 16 Hz, 18 Hz, 25 Hz and 43 Hz, the optimal result is achieved when the values of Moment 3, swing arm g thickness and driving rod 1 damping are 1300 N·mm, 8.7735 mm and 0.050, respectively, the amplitude displacement value of the actuator end reaches the optimal value, and the displacement values at 16 Hz, 18 Hz, 25 Hz and 43 Hz are 0.0879 mm, 0.01243 mm, 0.0983 mm and 0.0000 mm, respectively.

The displacement amplitude response curve of the execution end obtained after optimization is shown in Figure 23.

As shown in Figure 23, when the excitation frequency is 25 Hz, the amplitude of the execution end is the largest with a value of 0.0744 mm.

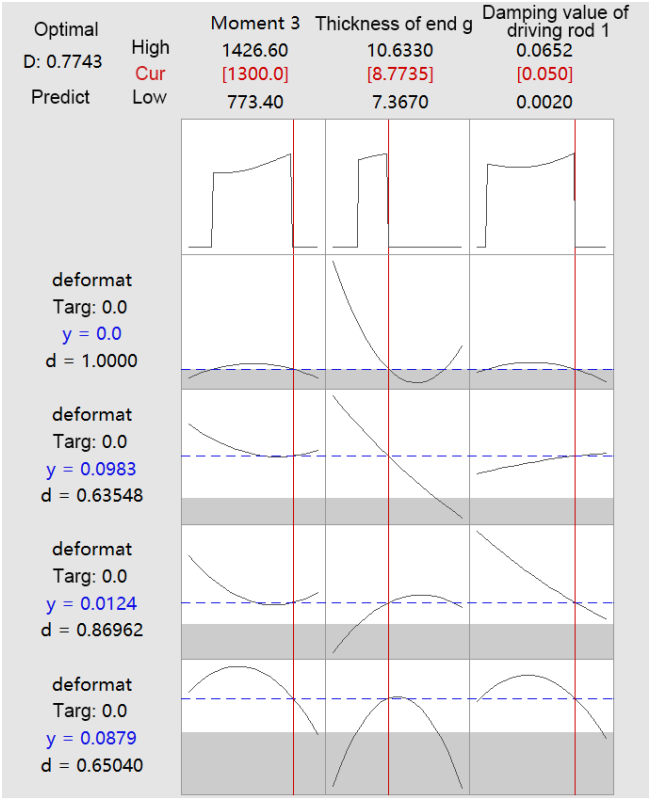


Figure 22. Optimization diagrams of coupling effects design.

Table 9. Optimization graph results of coupling effects design.

Response	Fitting Value	Fitting Value Error	95% Confidence Interval	95% Prediction Interval
Deformation (16 Hz)	0.0879	0.0257	(0.0297, 0.1461)	(−0.0227, 0.1985)
Deformation (18 Hz)	0.0124	0.0078	(−0.00518, 0.03004)	(−0.02103, 0.04588)
Deformation (25 Hz)	0.0983	0.0244	(0.0430, 0.1535)	(−0.0067, 0.2032)
Deformation (43 Hz)	0.0000	0.0119	(−0.0270, 0.0270)	(−0.0513, 0.0513)

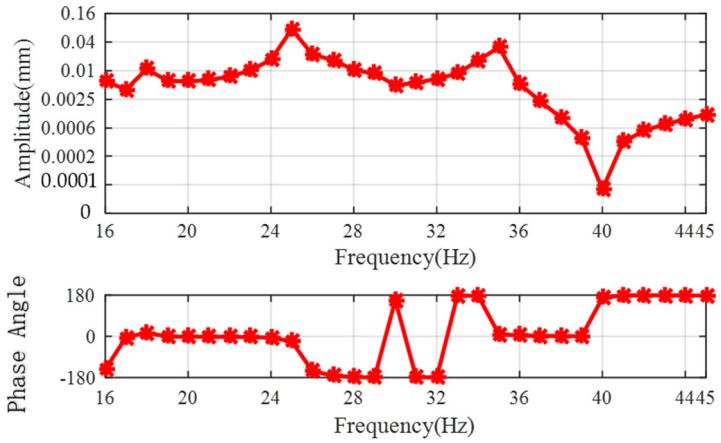


Figure 23. Amplitude response curve of the terminal surface after comprehensive optimization.

4. Conclusions

In this paper, a simulation model is established for the structural characteristics of a welding robot, and the correctness of the model is verified by the comparative analysis of a modal test and simulation results. The suppression resonance of a controllable mechanism welding robot end with a central composite design methodology is proposed. Considering the position of multiple excitation sources, member thickness and damping, the end vibration of the welding robot is optimized. In addition, the comparison of the end vibration response results before and after optimization verifies the effectiveness of the method proposed in this paper.

Author Contributions: Conceptualization, Y.H. and Y.S.; methodology, C.L.; software, Y.S.; validation, C.L.; formal analysis, Y.H.; writing—original draft preparation, Y.S.; writing—review and editing, Y.H.; visualization, Y.S. All authors have read and agreed to the published version of the manuscript.

Funding: This research was funded by the National Natural Science Foundation of China (NSFC) grant number [51575201].

Institutional Review Board Statement: Not applicable.

Informed Consent Statement: Not applicable.

Acknowledgments: This work was financially supported by the National Natural Science Foundation of China (NSFC) under grant number [51575201].

Conflicts of Interest: The authors declare no conflict of interest.

References

1. Wang, X.; Shi, Y.; Ding, D.; Gu, X. Double global optimum genetic algorithm–particle swarm optimization-based welding robot path planning. *Eng. Optim.* **2016**, *48*, 299–316. [CrossRef]
2. Yi, J.M.; Han, M. Welding robot welding process research and development of intelligent technology. *Appl. Mech. Mater.* **2013**, *419*, 774–777. [CrossRef]
3. Liu, C.; Wang, H.; Huang, Y.; Rong, Y.; Meng, J.; Li, G.; Zhang, G. Welding seam recognition and tracking for a novel mobile welding robot based on multi-layer sensing strategy. *Meas. Sci. Technol.* **2022**, *33*, 055109. [CrossRef]
4. Hong, L.; Huang, W.L. Vibration Test on Welding Robot. *Procedia Comput. Sci.* **2020**, *166*, 323–329. [CrossRef]
5. Zou, Y.; Lan, R. An end-to-end calibration method for welding robot laser vision systems with deep reinforcement learning. *IEEE Trans. Instrum. Meas.* **2020**, *69*, 4270–4280. [CrossRef]
6. Jiang, H.; Wu, C.; Chen, B. Vibration Suppression of Hub Motor-Air Suspension Vehicle. *Energies* **2022**, *15*, 3916. [CrossRef]
7. Sun, Z.; Zeng, Q.; Wan, L.; Dai, H. Control and Dynamic Characteristics Analysis for the Double-Compound Axial Piston Pump Based on Working Conditions. *Machines* **2022**, *10*, 411. [CrossRef]
8. Wu, X.; Liu, X.; Chen, J.; Liu, K.; Pang, C. Parameter Optimization and Application for the Inerter-Based Tuned Type Dynamic Vibration Absorbers. *Buildings* **2022**, *12*, 703. [CrossRef]
9. Cui, G.; Liu, J.; Hu, Z.; Zhang, Y.; Hou, H. Performance analysis and optimization of a rigid-flexible parallel manipulator. Proceedings of the Institution of Mechanical Engineers. Part C. *J. Mech. Eng. Sci.* **2020**, *234*, 4620–4635. [CrossRef]
10. Kawamura, S.; Iwamoto, Y.; Minamoto, H.; Kamigaki, T.; Taniyama, Y.; Kawamura, H. Structural deign optimization for a two-link robot to suppress undesirable vibration. *J. Adv. Mech. Des. Syst. Manuf.* **2009**, *3*, 289–298. [CrossRef]
11. Sevvel, P.; Satheesh, C.; Senthil Kumar, R. Generation of regression models and multi-response optimization of friction stir welding technique parameters during the fabrication of AZ80A Mg alloy joints. *Trans. Can. Soc. Mech. Eng.* **2020**, *44*, 311–324. [CrossRef]
12. Wang, X.; Xia, Z.; Zhou, X. Multiobjective path optimization for arc welding robot based on DMOEA/D-ET algorithm and proxy model. *IEEE Trans. Instrum. Meas.* **2021**, *70*, 1–13. [CrossRef]
13. Lu, Z.; Fan, J.; Hou, Z.; Deng, S.; Zhou, C.; Jing, F. Automatic 3D seam extraction method for welding robot based on monocular structured light. *IEEE Sens. J.* **2021**, *21*, 16359–16370. [CrossRef]
14. Shieh, C.J.; Liao, H.F.; Lee, C.C. Optimization of lipase-catalyzed biodiesel by response surface methodology. *Bioresour. Technol.* **2003**, *88*, 103–106. [CrossRef]
15. Tan, I.A.W.; Ahmad, A.L.; Hameed, B.H. Optimization of preparation conditions for activated carbons from coconut husk using response surface methodology. *Chem. Eng. J.* **2008**, *137*, 462–470. [CrossRef]
16. Wei, Z.J.; Liao, A.M.; Zhang, H.X.; Liu, J.; Jiang, S.T. Optimization of supercritical carbon dioxide extraction of silkworm pupal oil applying the response surface methodology. *Bioresour. Technol.* **2009**, *99*, 4214–4219. [CrossRef]

17. Ab Ghani, Z.; Yusoff, M.S.; Zaman, N.Q.; Zamri, M.F.M.A.; Andas, J. Optimization of preparation conditions for activated carbon from banana pseudo-stem using response surface methodology on removal of color and COD from landfill leachate. *Waste Manag.* **2017**, *62*, 177–187. [CrossRef]
18. Wong, K.H.; Li, G.Q.; Li, K.M.; Razmovski-Naumovski, V.; Chan, K. Optimisation of Pueraria isoflavonoids by response surface methodology using ultrasonic-assisted extraction. *Food Chem.* **2017**, *231*, 231–237. [CrossRef]
19. Li, Y.; Zhu, C.P.; Zhai, X.C. Optimization of enzyme assisted extraction of polysaccharides from pomegranate peel by response surface methodology and their anti-oxidant potential. *Chin. Herb. Med.* **2018**, *10*, 416–423. [CrossRef]
20. Tgarguifa, A.; Abderafi, S.; Bounahmidi, T. Energetic optimization of Moroccan distillery using simulation and response surface methodology. *Renew. Sustain. Energy Rev.* **2017**, *75*, 415–425. [CrossRef]
21. Fang, L.; Wu, B.; Chan, J.K.; Lo, I.M. Lanthanum oxide nanorods for enhanced phosphate removal from sewage: A response surface methodology study. *Chemosphere* **2018**, *192*, 209–216. [CrossRef]
22. Mostafaei, B.; Ghobadian, B.; Barzegar, M.; Banakar, A. Optimization of ultrasonic reactor geometry for biodiesel production using response surface methodology. *J. Agric. Sci. Technol.* **2018**, *15*, 697–708.
23. Dehghan, S.; Rezaei Kalantary, R.; Nazari, S.; Moradi, M.; Rastegar, A.; Shirzad Siboni, M. Optimization of dimethyl phthalate degradation parameters using zero-valent iron nanoparticles by response surface methodology: Determination of degradation intermediate products and process pathway. *J. Maz. Univ. Med. Sci.* **2018**, *27*, 194–216.
24. Vedrtnam, A.; Singh, G.; Kumar, A. Optimizing submerged arc welding using response surface methodology, regression analysis, and genetic algorithm. *Def. Technol.* **2018**, *14*, 204–212. [CrossRef]
25. Bae, J.H.; Park, Y.D.; Lee, M. Optimization of welding parameters for resistance spot welding of AA3003 to galvanized DP780 steel using response surface methodology. *Int. J. Automot. Technol.* **2021**, *22*, 585–593. [CrossRef]